MNRAS **000**, 000–000 (0000) Preprint 9 September 2019 Compiled using MNRAS LATEX style file v3.0

The Near and Mid-infrared photometric properties of known redshift $z \geq 5$ Quasars

Nicholas P. Ross* and Nicholas J. G. Cross
Institute for Astronomy, University of Edinburgh, Royal Observatory, Edinburgh, EH9 3HJ, United Kingdom

9 September 2019

ABSTRACT
We assemble a catalogue of 463 spectroscopically confirmed very high ($z \geq 5.00$) redshift quasars and report their near- ($ZYJHK_s/K$) and mid- (WISE W1234) infrared properties. 97% of the VHzQ sample is detected in one or more NIR ($ZYJHK/K_s$) band, with lack of coverage rather than lack of depth being the reason for the non-detections. 362 (78%) of the very high redshift quasars are detected at 3.4μm in the W1 band from the unWISE catalog and all of the $z \geq 7$ quasars are detected in both unWISE W1 and W2. Using archival WFCAM/UKIRT and VIRCAM/VISTA data we check for photometric variability that might be expected from super-Eddington accretion. We find 32 of the quasars have sufficient NIR measurements and signal-to-noise to look for variability. Weak variability was detected in multiple bands of SDSS J0959+0227, and very marginally in the Y-band of MMT J0215-0529. Two other quasars, SDSS J0349+0034 and SDSS J2220-0101 had significant differences between their WFCAM and VISTA magnitudes in one band. With supermassive black hole accretion likely to be redshift invariant up to very high-redshift, further monitoring of these sources is warranted. All the data, analysis codes and plots used and generated here can be found at: github.com/d80b2t/VHzQ.

Key words: Astronomical data bases: surveys – Quasars: general – galaxies: evolution – galaxies: infrared.

1 INTRODUCTION

Very high redshift quasars (VHzQ; defined here to have redshifts $z \geq 5.00$) are excellent probes of the early Universe. This includes studies of the Epoch of Reionization for hydrogen (see e.g. **??**, for reviews), the formation and build-up of supermassive black holes (e.g., **???????**) and early metal enrichment (see e.g., **???**).

Super-critical accretion, where $\dot{M} > \dot{M}_{\rm Edd}$, is a viable mechanism to explain the high, potentially super-Eddington, luminosity and rapid growth of supermassive black holes in the early universe (e.g., **???????**). Thus, one could expect VHzQs to potentially vary in luminosity as they go through phases of super-critical accretion. These signatures of photometric variability should be looked for, noting the rest-frame optical emission is redshifted into the observed near-infrared (NIR) at redshifts $z > 5$. Fortunately, data are now in place from deep, wide-field NIR instruments and surveys such as the Wide Field Camera (WFCAM) instrument on the United Kingdom Infra-Red Telescope (UKIRT) in the Northern Hemisphere and the VISTA InfraRed CAMera (VIRCAM) on the Visible and Infrared Survey Telescope for Astronomy (VISTA) in the Southern Hemisphere, that are necessary for identifying VHzQs.

Quasars are known to be prodigious emitters of infrared emission, thought to be from the thermal emission of dust grains heated by continuum emission from the accretion disc (e.g., **????**). Observations in the mid-infrared, e.g. ∼3-30μm allow discrimination between AGN[1] and passive galaxies due to the 1.6μm "bump" entering the MIR at $z \approx 0.8-0.9$ (e.g., **??????**) as well as between AGN and star-forming galaxies due to the presence of Polycyclic Aromatic Hydrocarbon (PAHs) at $\lambda > 3\mu$m (e.g., **??**).

? and **?** report on the discovery of a quasar without hot-dust emission in a sample of 21 $z \approx 6$ quasars. Such apparently hot-dust-free quasars have no counterparts at low redshift. Moreover, those authors demonstrate that the hot-dust abundance in the 21 quasars builds up in tandem with

* E-mail: npross@roe.ac.uk

[1] Historically, "quasars" and "Active Galactic Nuclei (AGN)" have described different luminosity/classes of objects. In recognition of the fact that both terms describe accreting supermassive black holes, we use these terms interchangeably, with a preference for quasar, since we are generally in the higher-L regime (e.g. **?**).

the growth of the central black hole. But understanding how dust first forms and appears in the central engine remains an open question (**??**).

WISE mapped the sky in 4 passbands, in bands centered at wavelengths of 3.4, 4.6, 12, and 23μm. The all sky 'AllWISE' catalogue release, contains nearly 750 million detections at high-significance[2], of which over 4.5M AGN candidates have been identified with 90% reliability (**?**). **?** presented WISE mid-infrared (MIR) detections of 17 (55%) of the then known 31 quasars at $z > 6$. However, **?** was compiled with the WISE 'All-Sky' data release, as opposed to the superior AllWISE catalogues. That sample only examined the 31 known $z > 6$ quasars; our sample has 170 objects with redshift $z \geq 6.00$ (with 108 detected in WISE). **?** reports WISE W1, W2, W3 and W4 magnitudes for the Panoramic Survey Telescope and Rapid Response System 1 (Pan-STARRS1, PS1; **??**), but with no further investigation into the reddest WISE waveband for the VHzQs.

Critically, we now have available to us new W1 and W2 photometry from the 'unWISE Source Catalog' (**?**), a WISE-selected catalogue that is based on significantly deeper imaging and has a more extensive modeling of crowded regions than the AllWISE release. For the first time in a catalogue, unWISE takes advantage of the ongoing mid-IR Near-Earth Object Wide-Field Infrared Survey Explorer Reactivation mission (NEOWISE-R; **?**), and achieves depths ∼0.7 mag deeper than AllWISE (in W1/2). This additional depth is a significant advantage in the detection and study of VHzQs in the 3-5 micron regime.

Here we present for the first time the combined near-infrared properties (from UKIRT and VIRCAM) and the new mid-infrared unWISE for all the spectroscopically known $z \geq 5.00$ quasars. Our motivations are numerous and include: *(i)* establishing the first complete catalogue of $z > 5.00$ quasars since the pioneering work from SDSS; *(ii)* utilizing all the WFCAM and VISTA near-infrared photometry available for the quasars; *(iii)* making the first study of near- and mid-IR variability of the VHzQ population and *(iv)* establishing the photometric properties for upcoming surveys and telescopes including the Large Synoptic Survey Telescope (LSST)[3], ESA *Euclid*[4] and the *James Webb Space Telescope* (JWST)[5,6,7,8]. We chose redshift $z = 5.00$ as our lower redshift limit due to a combination of garnishing a large sample, adequately spanning physical properties (e.g. luminosity, age of the Universe) and to highlight the parts of $L - z$ parameter space where $z > 5$ quasars still wait to be discovered.

This paper is organized as follows. In Section 2, we present the assembled list of the 463 $z \geq 5.00$ VHzQs that we have compiled. We then give a high-level overview of the photometric surveys and datasets we use and present the photometry of the VHzQs. In Section 3 we investigate the variability properties of the VHzQs, looking for evidence of super-critical accretion. In Section 4 we calculate how many $z > 5$ quasars we should expect to find in current datasets. We conclude in Section 5 and present all the necessary details to obtain our dataset in the Appendices.

[2] wise2.ipac.caltech.edu/docs/release/allwise/expsup/sec2_1.html
[3] lsst.org; [4] sci.esa.int/euclid; [5] jwst.nasa.gov; [6] sci.esa.int/jwst; [7] www.asc-csa.gc.ca/eng/satellites/jwst; [8] jwst.stsci.edu.

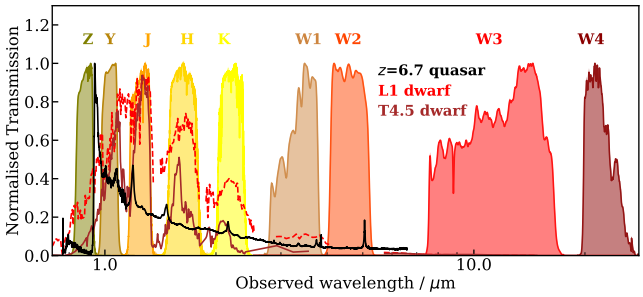

Figure 1. The spectral bands used in this paper. The $ZYJHK$ filter curves are from UKIRT/WFCAM. The $ZYJHK_s$ VISTA/VIRCAM filter curves are similar, but not identical to these. The WISE passbands W1-4 are presented, though without the **?** W4 recalibration. The quasar spectrum is a composite based on **?** and **?**. The L and T dwarf spectra are from **?**.

We present all our photometry and magnitudes on the AB system. For NIR, we use the **?** and **?** system which has a zeropoint of −48.60. For WISE, the AB-Vega offsets are calculated using the **?** AB system, which has a zeropoint of -48.574. So to remain on the -48.60 system, and assuming a flux density $F_\nu \propto \nu^0$, one needs to subtract 0.026 mag from the zeropoints: (ΔW1, ΔW2, ΔW3) = (2.673, 3.313, 5.148). For W4, we use the calibration of **?**, ΔW4= 6.66. These magnitudes are *not* Galactic extinction corrected.

We use a flat ΛCDM cosmology with $H_0 = 67.7$ km s^{-1} Mpc^{-1}, $\Omega_M = 0.307$, and $\Omega_\Lambda = 0.693$ **?** to be consistent with **?** and all logarithms are to the base 10.

2 METHOD AND DATA

Quasars are generally identified by photometric selection followed by spectroscopic confirmation. Here, we reverse this method obtaining first a list of spectroscopic quasars and then obtain photometric information.

We have compiled a list of **488** quasars with redshifts $z \geq 5.00$. We use all the $z \geq 5.00$ quasars that have been discovered, spectroscopically confirmed and published as of 2018 December 31 (MJD 58483). We then obtain optical, near-infrared and mid-infrared photometry for the spectral dataset. The near-infrared data comes from two sources: first, the WFCAM (**?**) on the UKIRT, primarily, but not exclusively, as part of the UKIRT Infrared Deep Sky Survey (UKIDSS; **?**). And second, data from the VIRCAM on the VISTA (**??**). The mid-infrared, $\lambda = 3 - 30\mu$m wavelength data is from the Wide-Field Infrared Survey Explorer (WISE; **??**) mission. For reference, Figure 1 displays the wavelength and normalised transmission of the filters in question.

2.1 Spectroscopy

We compile the list of all known, spectroscopically confirmed quasars from the literature. This list was complied from a range of surveys and papers. Specifically, we use data from: ????, ?, ?, ??, ?, ?, ?, ?, ??????, ?, ?, ????, ?, ?, ?, ?, ??, ??, ?, ?, ???, ?, ?, ??, ??, ??, ?, ?, ?, ?, ?, ??????, ????, ?????, ? ?? and ?.

We updated our list of objects between the submitted paper and accepted due to feedback from

Survey	# VHzQs	(%)	Survey reference
ATLAS	4	(0.86)	?
CFHQS	20	(4.32)	?
DELS[a]	16	(3.46)	?
ELAIS	1	(0.22)	?
FIRST	1	(0.22)	?
HSC	8	(1.73)	?
IMS	5	(1.08)	?
MMT	12	(2.59)	?
NDWFS	1	(0.22)	?
PSO	83	(17.93)	??
RD	1	(0.22)	?
SDSS	170	(36.72)	?
SDWISE[b]	27	(5.83)	?
SHELLQs	55	(11.88)	?
SUV[c]	20	(4.32)	?
UHS	1	(0.22)	?
ULAS	10	(2.16)	?
VDES[d]	17	(3.67)	?
VHS	1	(0.22)	?
VIK	9	(1.94)	?
VIMOS	1	(0.22)	?

Table 1. The source and number of the VHzQ, with the key survey reference also given. Recent survey name and acronyms include: [a]DESI Legacy Imaging Survey; [b]SDWISE = SDSS+WISE; [c]SUV = SDSS-ULAS/VHS; [d]VDES = VHS/VIKING+DES;

other scientists. We discuss these changes in detail in Appendix A.

Most of these objects are easily identified by their broad Lyα emission line, N v emission and characteristic shape blueward of 1215Å in the rest-frame. As we shall see, some of the recently discovered objects are close to the galaxy luminosity function characteristic luminosity M^*, and some have relatively weak or maybe even completely absorbed Lyα (e.g. Figures 7 and 10 in **?**). We leave aside detailed investigation and discussion into spectral features and line strengths, and take as given the published spectra and redshift identifications.

The breakdown of how many VHzQ each survey reports is given in Table 1. The Sloan Digital Sky Survey (SDSS) and the Pan-STARRS1 (PS1; PSO in Table 1) survey and alone identified over half (54.6%) of the VHzQ population. Data from the Hyper Suprime-Cam (HSC) on the Subaru telescope is responsible for 13.6% of our dataset (HSC+SHELLQs in Table 1). The combination of surveys is also vital for identifying VHzQs. The UKIDSS Large Area Survey (ULAS) on its own, or in combination with other surveys is responsible for 6.5% of the sample (SUV+ULAS) including the highest-z object. Where more than one survey is used for the high-redshift identification (e.g. via shorter-band veto and longer wavelength detection) we follow the discovery paper naming convention.

The redshifts for the VHzQs generally come from the measurement of broad UV/optical emission lines. There are far infra-red emission lines e.g. C ii 158 μm available for several objects, but at the level of our current analysis broadline redshifts are sufficient.

The number of objects at or above various redshifts, along with the corresponding age of the Universe is given in Table 2.

The $N(z)$ redshift histogram is given for the sample in Figure 2. We split the contribution up by survey. For clarity we show the individual surveys of SDSS, PS1, HSC, the ULAS detection, and tally the remaining surveys together ("various").

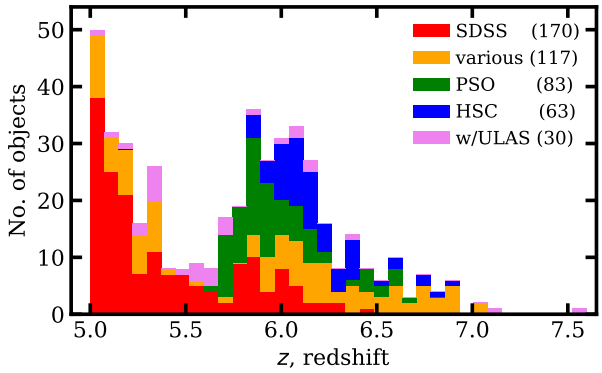

Figure 2. The redshift distribution $N(z)$ of the VHzQ sample. The bins are $\delta z = 0.075$ in width and have the data stacked on top of each other.

$z \geq$	Age / Myr	No. of objects
5.00	1180	463
5.70	1000	267
6.00	937	170
6.19	900	86
6.50	845	40
6.78	800	14
7.00	767	4
7.50	700	1

Table 2. The number of objects at or above a given redshift. The age of the Universe in Megayears is also given.

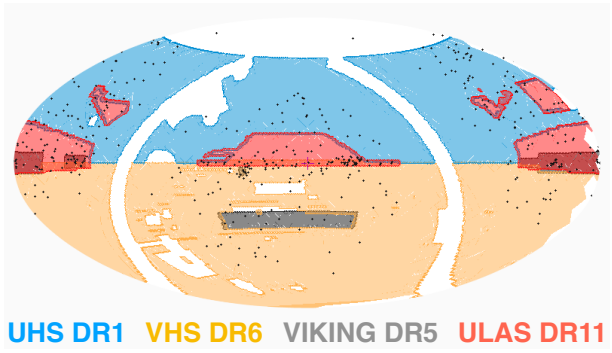

Figure 3. The coverage maps for VHS (DR6; orange), UHS (DR1; olive), VIKING (DR5; blue) and ULAS (DR11; red), the most recent public releases of the 4 main surveys. The VHzQs are given by black dots.

2.2 Near-infrared photometry

The near-infrared data in this paper comes from the Wide Field Astronomy Unit's (WFAU) Science Archives for UKIRT-WFCAM, the WFCAM Science Archive (WSA; **?**) and VISTA-VIRCAM, the VISTA Science Archive (VSA; **?**). These archives were developed for the VISTA Data Flow System (VDFS **?**).

We access both the WSA and the VSA and include

all non-proprietary WFCAM data, which covers all public surveys and PI projects from Semester 05A (2005-05-01) to 2017-Jan-01, and all non-proprietary VISTA data, which covers all public surveys and PI projects from science verification on 2009-Oct-15 to 2017-Jan-01.

Here we are not just querying the WSA or VSA data tables. We are taking a list of objects (positions) are performing matched aperture ("forced") photometry on the NIR imaging data. As such, we generate a set of tables that are different in subtle ways to the regular "Detection" tables. The two most important tables for our needs are the `[w/v]serv1000MapRemeasurement` and `[w/v]serv1000MapRemeasAver`.

We produce and provide a two new databases with all the necessary quantities and measurements to fully reproduce our tables, figures and results herein. Moreover, these databases report considerably more information than we report here. Full documentation can be found at the WSA Schema Browser and the VSA Schema Browser.

Figure 3 shows the areal coverage of the ULAS, UHS, VHS and VIKING. UHS DR1 is 12,600 deg^2 (J-band); ULAS DR1 3,700 deg^2 VHS DR6 16,000 deg^2 and VIKING DR5 is 1,300 deg^2. The overlap between UHS DR1 and VHS DR6 is 28 deg. These four surveys together cover 33,000 deg^2. VHS, ULAS and UHS do not observe in the Z-band.

2.2.1 Averaging matched photometry

The data was processed using a matched-aperture photometry method where flux is measured at the spectroscopic position of the quasar, without necessarily knowing if there is a formal detection in the NIR photometry beforehand. The matched-aperture pipeline is discussed in **?** and with fuller details to appear in a forthcoming paper (Cross et al., 2019, in prep).

We query the WSA and VSA performing matched-aperture photometry at the positions of our 463 VHzQs. This database is world-readable and we give the full recipe and relevant SQL queries for accessing both databases in Appendix **??** as well as online.

The photometry in a single epoch image often has low signal-to-noise. The advantage of matched aperture photometry on quasars is that co-adding is relatively simple if each epoch is taken in the same aperture and the aperture photometry has been corrected to total. Indeed, the standard aperture corrections work well for point sources. Coadding using the matched-aperture photometry can give better results for the photometry, where the individual epochs are taken from multiple projects with different field-centres and orientations and point-spread functions since the individual epoch scattered light, pixel distortion and aperture corrections can be applied with the correct weighting.

We average the aperture corrected calibrated fluxes (e.g. **aperJky3**), and then convert to magnitudes.

$$\bar{F} = \frac{\sum_i^N (w_i\, F_i)}{\sum_i^N w_i} \qquad (1)$$

where F_i is the i^{th} epoch measurement of a parameter to be averaged such as the aperture corrected calibrated flux in a $1''$ aperture (**aperJky3**) and $\bar{F}$ is the weighted mean average of this parameter. The weight for each epoch $w_i = 1/(\sigma_F)^2$ if the epoch is included and $w_i = 0$ if an epoch is excluded for quality control purposes. The weights of each epoch in each averaged catalogue are tabulated in the `[w]serv1000MapAverageWeights`.

We calculate a set of averaged catalogues, for each pointing and filter, based on the requirements in `RequiredMapAverages`, in these cases over time spans of 7, 14, 30, 91, 183 days, 365 days, 730 days, over 10 epochs and over all epochs. The averaging process starts at the first epoch and works onwards from there. Again, we present these measurements in the new SQL tables.

We detect 359 unique quasars in the WFCAM WSA database, 220 quasars are detected in the VISTA VSA database with 130 objects in common with both WFCAM and VISTA data. We give the necessary SQL queries syntax at `d80b2t/VHzQ`.

2.3 MIR data

The MIR data for this study comes from the Wide-field Infrared Survey Explorer (WISE) mission, and we utlize data from the WISE cryogenic and the Near-Earth Object WISE (NEOWISE; **?**) post-cryogenic and NEOWISE Reactivation Mission (NEOWISE-R **?**) survey phases.

We use data from the beginning of the WISE mission (2010 January; **?**) through the fifth-year of NEOWISE-R operations (**?**, 2018 December;). There are several major data releases and catalogues based on the WISE mission. Here we use two: the WISE AllWISE Data release and the recently released "unWISE Catalog" (**?**). The AllWISE program combines the W1 and W2 Single-exposure data from all the WISE survey phases (4-Band Cryo, 3-Band Cryo and Post-Cryo; 2010-01-07 thru 2011-02-01) survey phases, and the W3 and W4 from the 4-Band Cryo phase. The unWISE effort[9] is the unblurred coadds of the WISE imaging using the AllWISE and NEOWISE-R stacked data (**???**).

For the two shorter WISE bands, $\lambda_{\rm eff}3.37\mu$m W1 and $\lambda_{\rm eff}4.62\mu$m W2 we generally report the deeper, unblurred unWISE coadd data. For the two longer WISE bands, $\lambda_{\rm eff}12.1\mu$m and $\lambda_{\rm eff}22.8\mu$m we use the AllWISE Data Release. Most objects in the AllWISE Source Catalog are unresolved, so the best photometric measurements to use are the deep detection profile-fit photometry measures, `w`x`mpro`, `w`x`sigmpro` and `w`x`snr`. The unWISE Catalog absolute photometric calibration derives from the photometric calibration of the unWISE coadds (**?**), which is tied to the original WISE zero points through aperture fluxes in a 27.5" radius.

Previous works (e.g., **???**) found that cross-matches performed with a radius of 2-3" between the user catalogue and WISE was a good compromise between completeness and contamination (see e.g. Figure 4 of **?**). We thus use a cross-match radius of 2.75". When querying the AllWISE catalogues, "Cone Search Radius" in the AllWISE table search was set to 2.75" for the Spatial Constraints. The "One to One Match" was "not" checked; although possible, we consider it highly unlikely there would be more than one MIR source contributing to the flux of a single UV/optically bright rest-frame quasar. Investigating this in detail is very interesting but left to a future study.

[9] http://unwise.me

Knowing we have secure detections in the near-infrared bands, and wanting to boost the number of WISE W3/W4 detections, we allow ourselves to be less conservative in querying the AllWISE catalogues and also query the AllWISE Reject Table. However, with the exception of one object (SHELLQs J1208-0200), the AllWISE Reject Table does not contain any further W3/W4 detection information.

All fluxes in the unWISE catalog are reported there are in "Vega nanoMaggies", with the Vega magnitude of a source is given by

$$m_{\rm Vega} = 22.5 - 2.5\log(f), \tag{2}$$

where f is the source flux. The absolute calibration for unWISE is ultimately inherited from AllWISE through the calibration of **?**. This inheritance depends on details of the PSF normalization at large radii, which is uncertain. Subtracting 4 millimag from the unWISE W1, and 32 millimag from unWISE W2 fluxes improves the agreement between unWISE and AllWISE fluxes.

Thus to convert unWISE Vega magnitudes onto the AB system, we have:

$$\begin{aligned} {\rm W1}_{\rm AB,unWISE} &= 22.5 - 2.5\log(f_{\rm W1}) - 0.004 + 2.673 \\ {\rm W2}_{\rm AB,unWISE} &= 22.5 - 2.5\log(f_{\rm W2}) - 0.032 + 3.313 \end{aligned}$$

using the **?** AB system, and is slightly different to the transformations presented in **?**.

For the our MIR variability investigations, we use the NEOWISE-R 2019 Data Release. NEOWISE 2019 makes available the 3.4 and 4.6 m (W1 and W2) single-exposure images and extracted source information that was acquired up until 2018 December 13 (MJD 58465) including the fifth year of survey operations of NEOWISE. These fifth year NEOWISE data products are concatenated with those from the first four years into a single archive from 2013 December 13 (MJD 56639). The WISE scan pattern leads to coverage of the full-sky approximately once every six months (a"sky pass"), but the satellite was placed in hibernation in 2011 February and then reactivated in 2013 October. Hence, our light curves have a cadence of 6 months with a 32 month sampling gap.

Survey	QsoName	R.A. / deg (J2000)	Decl. / deg (J2000)	redshift	Y	J	H	K	unWISE W1	unWISE W2	AllWISE W3	AllWISE W4
PSO	J000.3401+26.8358	0.34011	26.83588	5.75	—	19.28 ± 0.062	—	—	18.949 ± 0.026	18.80 ± 0.050	17.74 ± 0.490	> 15.42
SDSS	J0002+2550	0.66412	25.84304	5.82	—	19.37 ± 0.069	—	—	18.919 ± 0.026	18.70 ± 0.047	17.56 ± 0.420	> 15.34
SDSS	J0005-0006	1.46808	-0.11550	5.85	—	20.73 ± 0.130	19.99 ± 0.086	20.54 ± 0.172	20.162 ± 0.079	19.98 ± 0.153	> 17.59	> 15.67
PSO	J002.1073-06.4345	2.10739	-6.43456	5.93	—	—	—	—	19.471 ± 0.044	19.24 ± 0.078	> 17.04	> 15.42
SDWISE	J0008+3616	2.21429	36.27041	5.17	—	19.33 ± 0.063	—	—	18.687 ± 0.021	18.71 ± 0.044	> 17.19	> 15.45
PSO	J002.3786+32.8702	2.37870	32.87026	6.10	—	20.99 ± 0.249	—	—	20.620 ± 0.106	—	—	—
SDSS	J0012+3632	3.13700	36.53781	5.44	—	19.01 ± 0.049	—	—	18.490 ± 0.017	18.51 ± 0.036	17.15 ± 0.230	15.35 ± 0.330
SDSS	J0017-1000	4.31117	-10.01540	5.01	—	—	—	—	18.645 ± 0.022	18.60 ± 0.045	17.17 ± 0.330	> 15.18
PSO	J004.3936+17.0862	4.39361	17.08630	5.80	—	20.74 ± 0.081	—	20.28 ± 0.092	20.503 ± 0.103	19.98 ± 0.145	—	—
PSO	J004.8140-24.2991	4.81408	-24.29916	5.68	—	—	—	—	18.989 ± 0.028	18.96 ± 0.061	17.27 ± 0.340	> 15.48
VDES	J0020-3653	5.13112	-36.89495	6.90	—	20.42 ± 0.068	—	19.32 ± 0.077	19.536 ± 0.041	19.69 ± 0.102	> 17.83	> 15.00
SDSS	J0023-0018	5.87779	-0.31011	5.06	—	20.39 ± 0.102	20.12 ± 0.126	19.94 ± 0.106	19.518 ± 0.046	19.41 ± 0.092	> 17.02	> 15.15
PSO	J006.1240+39.2219	6.12404	39.22193	6.62	—	21.28 ± 0.422	—	—	20.033 ± 0.064	—	—	—
SDWISE	J0025-0145	6.36183	-1.75903	5.07	18.03 ± 0.014	17.95 ± 0.014	17.72 ± 0.019	17.59 ± 0.018	17.520 ± 0.009	17.51 ± 0.018	16.54 ± 0.220	> 15.17
PSO	J007.0273+04.9571	7.02733	4.95712	6.00	20.33 ± 0.056	20.23 ± 0.074	20.29 ± 0.108	20.19 ± 0.105	19.847 ± 0.060	19.89 ± 0.135	> 17.40	> 14.98
SDWISE	J0031+0710	7.85775	7.17692	5.33	20.03 ± 0.082	20.20 ± 0.146	19.49 ± 0.106	19.61 ± 0.123	19.327 ± 0.039	18.96 ± 0.063	> 17.34	> 15.06
CFHQS	J0033-0125	8.29750	-1.42358	6.13	—	21.41 ± 0.190	21.32 ± 0.265	20.79 ± 0.169	20.874 ± 0.142	—	—	—
SDSS	J0034+3759	8.55979	37.99833	5.63	—	19.70 ± 0.091	—	—	19.149 ± 0.029	19.01 ± 0.056	> 17.18	> 15.76
PSO	J009.3573-08.1190	9.35733	-8.11902	5.72	—	—	—	—	19.489 ± 0.042	19.48 ± 0.095	> 17.34	> 15.02
DELS	J0038-1527	9.65042	-15.45656	7.02	—	—	—	—	19.410 ± 0.041	19.59 ± 0.104	> 17.45	> 15.36
PSO	J009.7355-10.4316	9.73551	-10.43164	5.95	—	—	—	—	19.160 ± 0.032	19.00 ± 0.061	> 17.35	> 15.07
PSO	J011.3899+09.0325	11.38987	9.03249	6.42	21.04 ± 0.234	—	20.64 ± 0.177	20.76 ± 0.251	20.442 ± 0.104	—	> 17.13	> 15.44
CFHQS	J0050+3445	12.52777	34.75601	6.25	—	19.97 ± 0.120	—	—	19.250 ± 0.033	18.99 ± 0.055	> 18.08	> 15.96

Table 3. The first 23 (i.e. 5%) of 463 very high-z quasars in Right Ascension order with near and mid-infrared photometry. The full table can be found here. The AB magnitude system is used with the WISE Vega to AB offsets being (ΔW1, ΔW2, ΔW3 ΔW4)=(2.669, 3.281, 5.148, 6.66) Since none of the first 23 objects have Z-band detections, we don't report that column here (but is reported in the main table). WISE AllWISE W3 and W4 values without formal errors are low-SNR detections.

Selection	number detected (%)
Any band ($ZYJHK/K_s$)	449 (97.0)
Z-band	75 (16.2)
Y-band	273 (59.0)
J-band	447 (96.5)
H-band	269 (58.1)
K or Ks-band	322 (69.5)

Table 4. Detection rate of VHzQs in the near-infrared. For the 14 objects that have no NIR detections, 3 have been observed but are not in our queried time range, 6 have not been observed yet and 5 objects are too far north to be visible by UKIRT.

abs(VIRCAM - WFCAM)	millimags	no. of objects
Z	23.2	3
Y	57.3	53
J	2.1	106
H	45.8	96
K_s/K	25.2	110

Table 5. Comparing the magnitudes in different WFCAM/UKIRT and VIRCAM/VISTA near-infrared bands.

$z \geq$	unWISE		AllWISE	
	W1	W2	W3	W4
5.00	362 (78.2%)	308 (66.5%)	51 (11.0%)	10 (2.2%)
5.70	186 (69.4%)	151 (56.3%)	15 (5.6%)	2 (0.7%)
6.00	109 (63.7%)	91 (53.2%)	8 (4.7%)	2 (1.2%)
6.19	63 (72.4%)	47 (54.0%)	3 (3.4%)	2 (2.3%)
6.50	34 (85.0%)	26 (65.0%)	1 (2.5%)	2 (5.0%)
6.78	12 (85.7%)	9 (64.3%)	0 (0.0%)	0 (0.0%)
7.00	4 (100.0%)	4 (100.0%)	0 (0.0%)	0 (0.0%)
7.50	1 (100.0%)	1 (100.0%)	0 (0.0%)	0 (0.0%)

Table 6. Detection rates in the mid-infrared bands from WISE as a function of redshift. A signal-to-noise cut of `wxsnr`> 3.0 has been used for each band.

3 RESULTS

Having collated the sample of 463 VHzQs, and obtained their near- and mid-infrared photometry we report here the various photometric properties of the quasars. Table 3 represents the culmination of this effort, *is the main data product of this paper* and we now exam the assembly of its contents in more detail.

First, we will concentrate on detection rate in the infrared, go on to report on the colour-redshift and colour-colour properties of our sample. We also investigate the photometric variability.

3.1 Detection Rates in the NIR

Table 4 gives the detection rates for the VHzQs in the NIR $YJHK/K_s$-bands. The first thing to note is that the coverage of the NIR surveys for example from the UKIDSS LAS and VISTA VHS, does not overlap the full area for where the VHzQs are detected.

There are 14 objects that have no NIR detections. 3 of these (PSOJ053.9605-15.7956, PSO J056.7168-16.4769 and DELSJ0411-0907) have been observed (by VHS) but are out of our queried time range (for which the data is publicly available). 6 objects are at declination $\delta < 0$ deg and have not been observed (or at least the data is not in the VSA archive yet). 5 objects are at a declination $\delta \geq +60$ deg are too far north for UKIRT and cannot be observed.

We note that although we are often working close to the magnitude limits of the surveys, Eddington bias is not a significant effect on our measurements, since we are not discovering new sources, but measuring properties of already known quasars. Indeed in the NIR WFCAM/VISTA data, using forced photometry reduces the Eddington bias to negligible levels since a flux will be measured regardless of whether the source is just bright enough (or too faint) to be detected above the background noise.

3.1.1 Comparing WFCAM and VISTA

There are 130 quasars observed in the overlapping area between WFCAM and VISTA. We used the `VegaToAB` values to put these objects on the same AB system, and for each object compared the two measurements. First, we calculated the weighted average (calibrated flux) in each filter of both and calculated the ratio and difference between each measurement and the average. Then for each filter we calculated the weighted average of the differences (in mag) for each instrument to see if there were significant offsets. The results are given in Table 5. The only filter with a significant offset is the Y-band. All of the VISTA averages are negative and all of the WFCAM ones are positive. The Ks versus K band comparison may be affected the different shapes of the filters, with K being significantly wider than K_s, able to detect light at longer wavelengths.

We have also checked for quasars with large differences in magnitude between the WSA and VSA. Objects were selected where the average flux was $> 0.$ and > 5 average flux error. In order to account for large errors in either the WFCAM or VISTA photometry, objects with δmag$< 2\times \sigma_{\delta\mathrm{mag}}$ in either WSA or VSA were removed. This selects two quasars with large, δmag > 0.2mag differences between the WSA and VSA. These are SDSSJ0349+0034 and SDSSJ2220-0101. For SDSSJ0349+0034 has a WSA K-band magnitude of 19.13 ± 0.24, while for the VSA K_s-band this is 18.36 ± 0.10 mag. For SDSSJ2220-0101, in J-band WSA $= 22.23\pm0.15$, for the VSA $= 19.38\pm0.04$.

3.2 Detection Rates in the MIR

Unlike the NIR coverage, the WISE satellite and mission performed an all-sky survey, so the location of every VHzQ in our dataset is covered. However, the depth of the WISE survey depends heavily on sky location, with locations near the Ecliptic Poles having the highest number of exposures.

Before reporting on the detection rates, we investigate this effect using the AllWISE Source Catalog. Figure 4 shows the WISE AllWISE magnitude versus signal-to-noise, colour coded by `wxcov` the mean coverage depth, in each corresponding band. The `w123cov` values are the mean pixel coverage in W1/2/3 from the W1/2/3 Atlas Tile Coverage Map within an aperture of circular area with a radius of 8.25" centered on the position of this source. For `w4cov` this radius is 16.5" (the AllWISE Source Catalog Column Descriptions has further details). The `wxcov` value takes into account

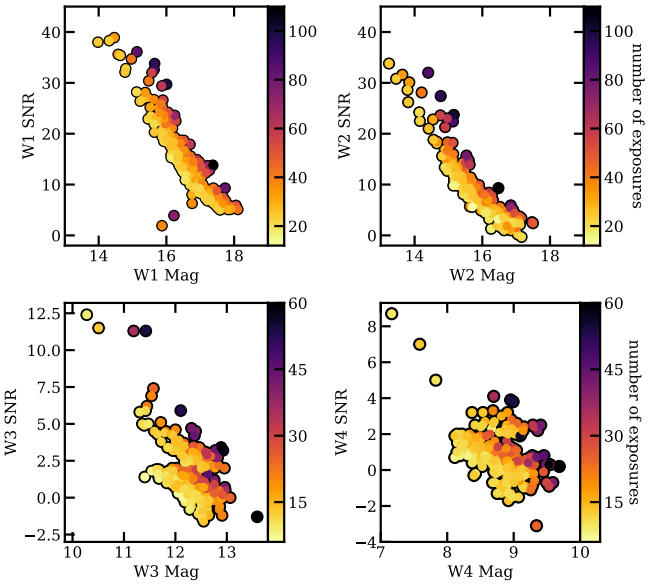

Figure 4. WISE W1/2/3/4 `wxmpro` Vega magnitude against signal-to-noise, colour coded by `wxcov` the mean coverage depth, in each corresponding band.

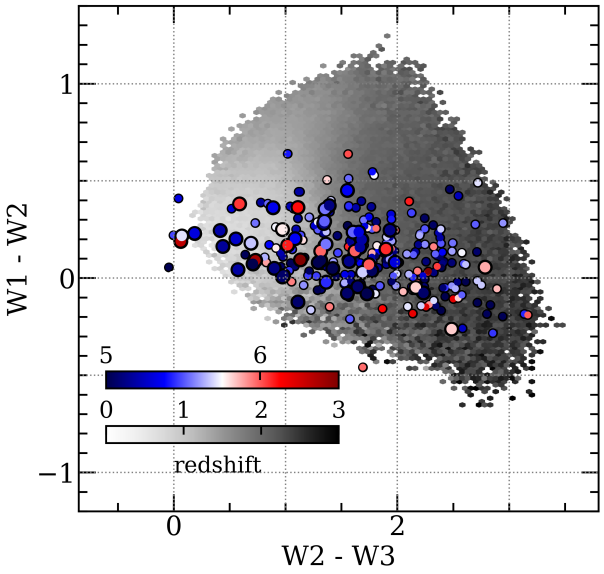

Figure 5. The (W2-W3) vs. (W1-W2) colour colour diagram showing the WISE colours for the 283 VHzQ that have reported w3mpro values (blue to red coloured points). 400,000 quasars at redshift $z \lesssim 3.0$ from the SDSS DR14 quasar catalogue (**?**) are also shown (grey colour-scale).

e.g., individual pixels in the measurement area that may be masked or otherwise unusable (reducing the effective pixel count and thus the mean coverage value) as well as pixels that are affected by distortions across the across the focal plane in single-exposure images (where this distortion is corrected when coadding to generate the Atlas Images).

In the two shorter bands W1/2 we see the clear and expected trend for brighter objects to have larger SNR, and also for the higher signal to noise for objects with more exposures at a given magnitude. The behaviour for the W3/4 bands is different, with two populations clearly evident in W3 and although a bit more mixed, also in W4. With the suggested split at SNR> 2, and no obvious R.A./Declination dependence seen, this behaviour is explained by the fact that there are non-detections in W3/4 for objects (with high W1/2 SNR) that are reported in the AllWISE catalogue.

Table 6 gives the detection rates for the VHzQs in the MIR WISE W1-4 bands. The unWISE depths are impressive with nearly 80% of all the VHzQs being detected in unWISE W1. 12 out of 14 (86%) in unWISE W1 (9 our of 14; 64% in unWISE W2) of the $z \geq 6.78$ quasars are detected and moreover *all of the* $z \geq 7$ *quasars are detected in both unWISE W1 and W2*. This bodes very well for future, small mirror infrared missions (e.g. **?**).

? present an all-sky sample of ≈1.35 million AGN meeting a two-color, (W1-W2) vs. (W2-W3), photometric selection as applied to sources from AllWISE. This colour-selection is motivated by **?**. We investigate if this catalogue, which is tuned for, and noted to be highly complete at, lower, $z \lesssim 2$ redshifts, contain the VHzQs. We find only 5 VHzQs from our sample match the Secrest catalogue, but given a W3 detection is required, this is not surprising. Further, in addition to the relative lack of sensitivity in W3, the mid-IR colors are moving out of the **?** color criterion at high redshift. This was shown using an AGN SED where AGNs above a redshift of about ∼2 fall out of the colour criterion, see e.g. Figure 5 of **?** and Figure 9 of **?**. **?** released two large catalogues of AGN candidates identified across 30,000 deg^2 of extragalactic sky from the WISE AllWISE Data Release. The "R90" catalogue, contains 4.5M AGN candidates at 90% reliability (≈150 AGN candidates per deg^2) while the "C75" catalogue consists of 20.9M AGN candidates at 75% completeness (≈700 AGN candidates per deg^2). Cross-matching our catalogue of 463 VHzQs with these catalogues, produces 42 matches with the R90 sample and 98 matches with the C75 sample. Both catalogues unsurprisingly match to the ultraluminous quasar SDSS J0100+2802 (**?**) while the C75, but not the R90 catalogue matches to the first redshift $z > 7$ quasar ULAS J1120+0641 (**?**). Neither the R90 or C75 catalogue matches to the current highest-redshift object J1342+0928 (**?**).

3.3 MIR Colours

Due to the depth all-sky coverage of the WISE (and NEOWISE-(R)) mission, several investigations have looked at how WISE detects AGN (e.g **????????**)

Figure 5 shows the (W1-W2) vs. (W2-W3) colour-colour diagram for the 283 VHzQs that have reported `w3mpro` values (blue to red coloured points), though we note that only 51 (18%) of these objects have `w3snr` >3.0. Approximately 400,000 quasars at redshift $z \lesssim 3.0$ from the SDSS Quasar Catalog using the Fourteenth data release (DR14Q; **?**) are also shown (grey colour-scale).

The VHzQ with the bluest colour in (W1-W2) is DELS J1048-0109, with (W1-W2) = -0.458 (i.e. 0.154 in Vega), and the WISE W1W2W3 color image is shown in Fig. 6 *(a)*. The reddest object in (W1-W2) is SHELLQs J2223+0326 with (W1-W2) = 0.719 (1.33 Vega).

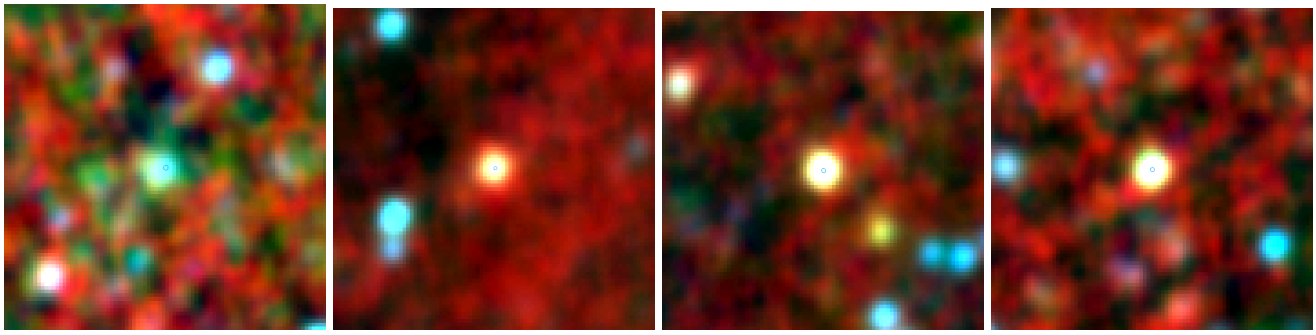

Figure 6. VHzQs with interesting MIR properties. The thumbnails are the RGB colour outputs using the AllWISE W1W2W3 bands from the IRSA WISE Image Service, with a scale of 120" on the side. *(a)* DELS J1048-0109 is the bluest in (W1-W2) colour quasar. *(b)* UHS J0439+1634 was discovered by **?** and is a strongly lensed quasar at $z = 6.51$. *(c)* SDWISE J0306+1853 has `w3mpro` $= 15.66 \pm 0.1$ (AB) and `w4mpro` $= 14.25 \pm 0.16$ (AB). *(d)* SDSS J0100+2802 is the **?** object.

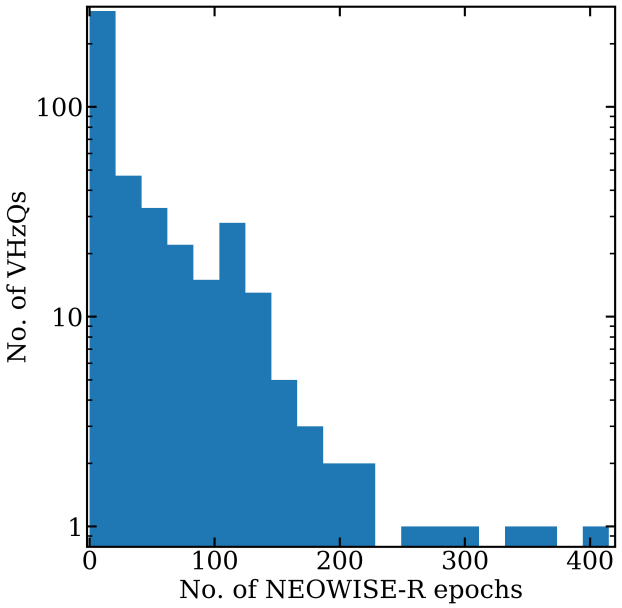

Figure 7. Histogram showing the total number of exposures for each detected VHzQ from the full combination of AllWISE, NEOWISE and NEOWISE-R.

The set of VHzQ detected in WISE W3 and W4 contains 51 objects that are detected in the broad W3 filter and 10 objects that are formally detected in W4 (`w4snr`$\geq$3.0). Three of the W3/4 objects are presented in Figure 6. UHS J0439+1634 (Fig. 6 *(b)*) with W4=7.165±0.12 was discovered by **?** and is a strongly lensed quasar at z =6.51. This high luminosity is mostly not intrinsic, but is boosted by an intervening redshift z ∼0.7 galaxy. Other high-redshift quasars that are bright W3/4 objects e.g. SDWISE J0306+1853 (Fig. 6 *(c)*) may well also so be lensed (e.g., **???**), but high-resolution follow-up is needed to confirm. SDSS J0100+2802 (redshift $z = 6.33$; Fig. 6 *(d)*) does not have a formal W4 detection (`w4snr`=2.4), but as reported by **?**, has a detection in the 2MASS J, H and K_s bands and is also the bluest object in both (W1-W3) and (W2-W3).

3.4 Variability

VHzQs, if accreting at, or above the Eddington limit, might well have changing mass accretion rates, i.e., $\dot{m}_{\rm accr}$. A consequence of this would be that these quasars exhibit signs of variability, most likely showing up in their UV/optical rest-frame emission. We look for evidence of this variability signature in the NIR and MIR light-curves of the VHzQs.

Quasars are known to have dramatically changing Balmer lines, especially Hβ (e.g., **????????????**). As a guide, we note that Hα is redshifted to 3.94μm (i.e. W1) at $z = 5.00$ and 5.57μm, which is between the W2 and W3-bands at $z = 7.50$. Hβ is redshifted to 2.92μm, which is the blue edge of W1, at $z = 5.00$ and 4.13μm at $z = 7.50$. Less well understood is the temporal behaviour of the metal lines, in particular C IV and Mg II . C IV enters the Y-band at redshift z=5.32 and exits at z=5.99, and enters the J-band at redshift $z = 6.55$ and exits at z=7.57. Mg II enters the H-band at redshift $z = 4.33$ and exits at $z = 5.37$ and enters the K-band at redshift $z = 6.25$ and exits at 7.50.

One key point to note is that the NEOWISE-AllWISE match radius is 3.00" and the AllWISE (and 2MASS) source information included in the NEOWISE Source Database are associations not identifications.

Figure 7 gives the number of NEOWISE-R epochs and detections for each VHzQ. There are 60 quasars with over 100 NEOWISE-R epochs, nine with over 200 epochs and four with over 300. Figure 8 presents three examples of the brighter MIR objects with well-sampled MIR lightcurves and associated colour changes; SDSS J0100+2802 (Fig. 8 top), SDWISE J1752+5036 (middle), SDSS J1621+5155 (bottom). For the light curves, we show weighted means for every 6 month NEOWISE-R scan. Due to the WISE scanning pattern, objects close to the North Ecliptic Pole are well sampled, and indeed this is the area for further investigation time-domain investigation with upcoming large infrared space telescopes (**??**).

Using the extended datasets described in Section 2.2, we select objects with at least 8 measurements observed with intervals of at least 30 days, in at least one filter. The the average calibrated flux over all epochs must be $>$ 0 (i.e. `aperJky3`$>$ 0) with the signal-to-noise is required to be $\geq$ 8 (i.e. `aperJky3/aperJky3Err`$\geq$8). With these criteria, there are 21 WFCAM and 12 VISTA objects with 1 object (VIK

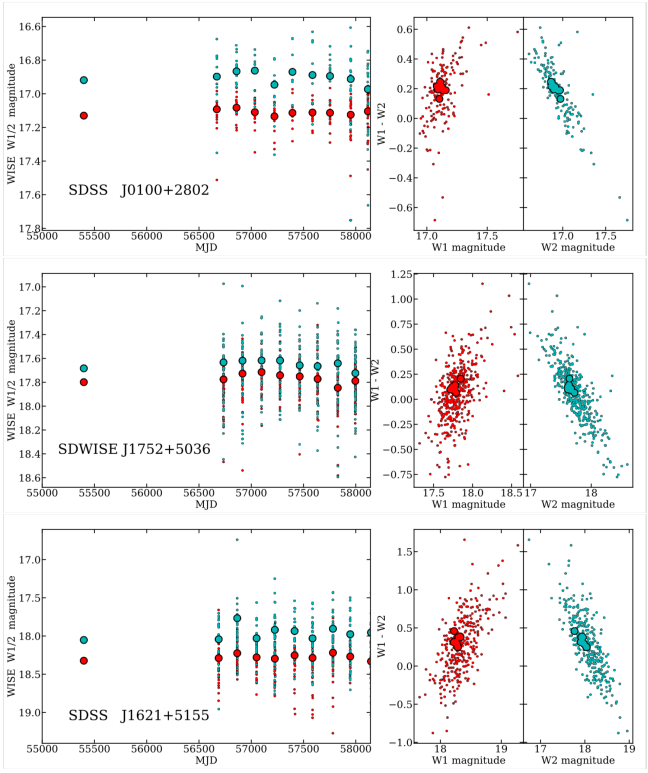

Figure 8. Here we show the MIR NEOWISE-R for SDSS J0100+2802 (top), SDWISE J1752+5036 (middle), and SDSS J1621+5155 (bottom). Red points are the W1 band; cyan points the W2 band. For the light curves, we show weighted means for every 6 month NEOWISE-R scan.

J1148+0056) in common to both, and this sample of 32 is our starting point for variability investigations.

The clipped median and median absolute deviation is then calculated

$$var = 1.48 \times \text{m.a.d.}/\bar{\epsilon} \quad (3)$$

where var is the index of variation, m.a.d. is the median absolute deviation, and $\bar{\epsilon}$ is the mean of the error in each point in the light curve, divided by the total number of points. We apply the criteria $var >= 3.$ to light-curves from the original measurements and also to light-curves where measurements have been averaged over different time-scales to improve the signal-to-noise. We found that two quasars showed signs of variability: MMT J0215-0529 (see Fig. 9) in the Y-band with an average time-scale of 30 days and amplitude of 0.3 mag, and SDSS J0959+0227 (see Fig. 12) in the Y and H-bands, with timescales of 1 year or 6 months for Y only. The H-band amplitude was 0.9 mag and the Y-band amplitude was 1.2 mag if averaged over 6 months, or 0.9 mag if averaged over 1 year.

We present four objects that are particularly well-sampled in the NIR. These are: MMT J0215-0529 (z = 5.13; Figure 9), CFHQS J0216-0455 (z = 6.01; Figure 10), SHELLQs J0220-0432 (z = 5.90; Figure 11) and SDSS J0959+0227 (z = 5.07; Figure 12). We incorporate the MIR NEOWISE-R light curve data where available.

We note that sometimes the average flux is negative and so a default magnitude is reported. This is apparent

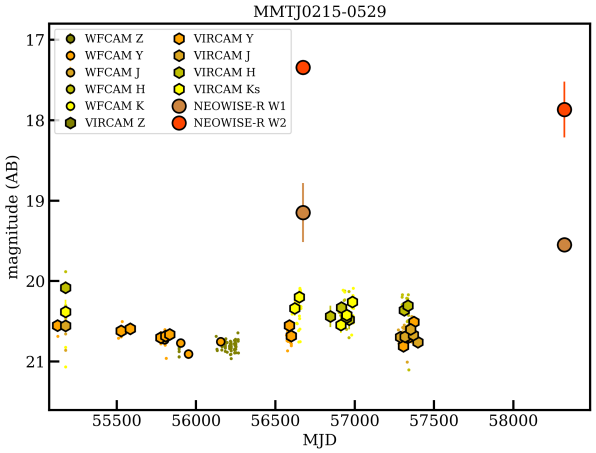

Figure 9. The infrared light curve for MMT J0215-0529 with data from WFCAM (smaller solid circles), VIRCAM (hexagons) and NEOWISE-R (larger solid circles). MMT J0215-0529 was identified by **?**,

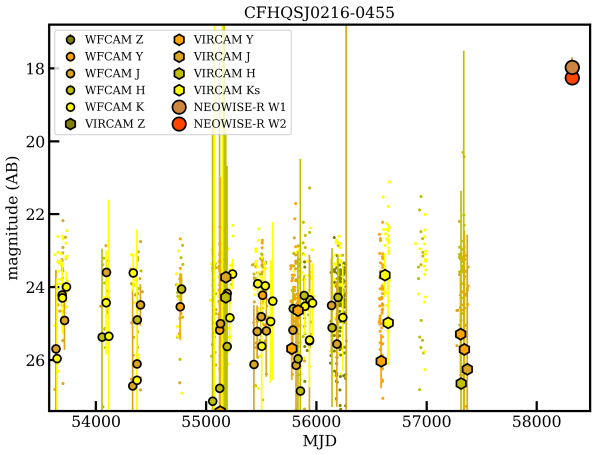

Figure 10. The same as Fig. 9 except for CFHQS J0216-0455.

for the average H and K_s flux for CFHQS J0216-0455 at MJD=56900. Interestingly this is evident in both the H and K_s filters, but with this quasar not much brighter than the detection limit, one must be very careful with any (over) interpretation.

Even with well sampled data across the 3000-4000 day observed time-scales that the WFCAM and VISTA surveys span, the $(1 + z)$ time-dilation dramatically affects the sampled rest-frame timescales sampled, which are ∼300-700 days. Indeed, when sharp changes in a accretion rate are expected on the system's dynamical timescale of several kilo-years (e.g., **?**), then seeing any variability signature is not expected. However, noting that *(i)* accretion onto supermassive black holes should be generally time invariant, and *(ii)* that in lower redshift quasars, which also have massive $>10^8$ $M_\odot$ black holes, dramatic changes in both continuum and

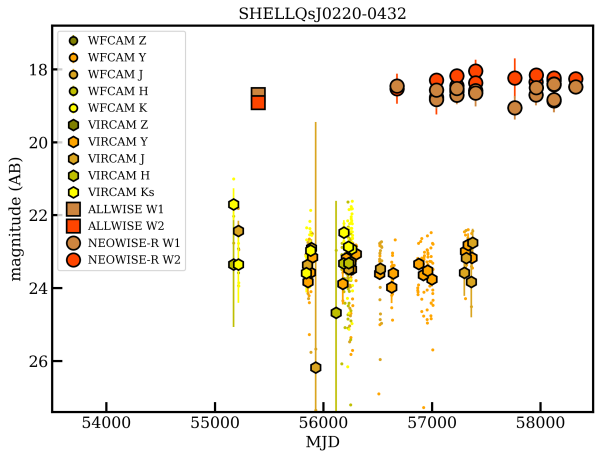

Figure 11. The same as Fig. 9 except for SHELLQs J0220-0432.

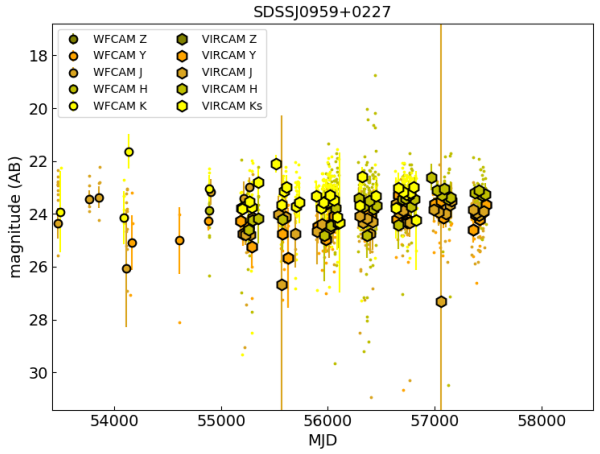

Figure 12. The near infrared light curve for SDSS J0959+0227. Note, SDSS J0959+0227 is too faint in the MIR to be detected by AllWISE or unWISE.

line emission *is seen* on much shorter timescales, continued monitoring of these objects is definitely warranted.

We finally focus on SDSS J0959+0227 which is presented in **?** but is first reported in **?** as CID-2220 and a high-redshift, $z > 3$ AGN, in the Chandra-COSMOS field. The spectrum from this object is presented in **?** and shows SDSS J0959+0227 having a narrow Lyα line, and would likely be a Lyman-α emitting galaxy had it not been an X-ray source, The X-ray luminosity is $\approx 3\times10^{44}$ erg s^{-1} in the 2-10 keV rest-frame, so it is an AGN. This object is clearly not a regular broadline "Type 1" AGN. Noting that the redshift of $z = 5.07$ for SDSS J0959+0227, the Y, J, H, Ks/K-bands correspond to rest-wavelengths of $\sim$1690, 2055, 2690, 3515/3625Å i.e. the rest-frame UV/very blue, so, so the regular blue QSO continuum could be emerging Thus, with the slightest hint of variability, this could potentially be a high-z AGN transitioning from a narrow-line "Type 2" object to a broadline Type 1 quasar.

4 CONCLUSIONS

In this study, we have, for the first time, compiled the list of all $z > 5$ spectroscopically confirmed quasars. We have assembled the NIR ($Z, Y, J, H, K/K_s$) and MIR (WISE W1/2/3/4) photometry for these objects and given their detection rates. We find that:

- SDSS and Pan-STARRS1 together identified over half of the VHzQ sample;
- There remains a quasar "redshift desert" at $z \approx 5.3 - 5.7$, though efforts are being made to address this (e.g., **?**);
- 97.0% of the VHzQ sample is detected in one or more NIR ($ZYJHK/K_s$) band;
- The 14 objects that are not detected in the NIR are due to lack of coverage rather than lack of depth;
- 362 (78.2%) VHzQs are detected by WISE, e.g. in the deeper unWISE W1 catalog.
- All of the $z \geq 7$ quasars are detected in both unWISE W1 and W2.
- 32 of the quasars had enough NIR measurements and sufficient NIR measurements and signal-to-noise to look for variability. Weak variability was detected in multiple bands of SDSS J0959+0227, and very marginally in the Y-band of MMT J0215-0529. 2 other quasars, SDSS J0349+0034 and SDSS J2220-0101 had significant differences between their WFCAM and VISTA magnitudes in one band, also indicating variability.

The science reach of $z > 5$ quasars will continue to be important well into the next decade (**???**) and will provide key insights into direct collapse black holes, hydrogen reionization and the physics of accretion in the first $\lesssim$700 million years of the Universe.

Author Contributions

N.P.R. initiated the project, compiled the list of $z > 5.00$ quasars, wrote most of the analysis code, developed the plotting scripts, and developed and wrote the initial and subsequent drafts of the manuscript.

N.J.G.C. supplied the critical near-infrared expertise and database for which the bulk of the project relies. N.J.G.C. also contributed directly to the writing of the manuscript.

Availability of Data and computer analysis codes

All materials, databases, data tables and code are fully available at: https://github.com/d80b2t/VHzQ

ACKNOWLEDGEMENTS

NPR acknowledges support from the STFC and the Ernest Rutherford Fellowship scheme.

We thank:

◦ Mike Read at the ROE WFAU for help with the WFCAM Science Archive (WSA) and the VISTA Science Archive (VSA).
◦ Aaron Meisner and Eddie Schlafly for facilitating early access to the unWISE Catalog.
◦ Tim Brooke at the IRSA Help Desk;
◦ Bernie Shiao at STScI for help with the Pan-STARRS1 DR1 CasJobs interface.
◦ Michael Cushing for supplying the Late Type stellar spectra and Beth Biller for useful discussion.
◦ Nathan Secrest for useful discussions on the mid-IR AGN catalogues.
◦ Krisztina Perger at for discussions about the input catalogue.

This paper heavily used TOPCAT (v4.4) (**??**). This research made use of `Astropy`, a community-developed core Python package for Astronomy (**??**).

The VISTA Data Flow System pipeline processing and science archive were used for the WFCAM and VISTA near infrared data are described in Irwin et al (2004), Hambly et al (2008) and Cross et al. (2012).

The Pan-STARRS1 Surveys (PS1) and the PS1 public science archive have been made possible through contributions by the Institute for Astronomy, the University of Hawaii, the Pan-STARRS Project Office, the Max-Planck Society and its participating institutes, the Max Planck Institute for Astronomy, Heidelberg and the Max Planck Institute for Extraterrestrial Physics, Garching, The Johns Hopkins University, Durham University, the University of Edinburgh, the Queen's University Belfast, the Harvard-Smithsonian Center for Astrophysics, the Las Cumbres Observatory Global Telescope Network Incorporated, the National Central University of Taiwan, the Space Telescope Science Institute, the National Aeronautics and Space Administration under Grant No. NNX08AR22G issued through the Planetary Science Division of the NASA Science Mission Directorate, the National Science Foundation Grant No. AST-1238877, the University of Maryland, Eotvos Lorand University (ELTE), the Los Alamos National Laboratory, and the Gordon and Betty Moore Foundation.

This project used data obtained with the Dark Energy Camera (DECam) and the NOAO Data Lab, The Data Lab is operated by the National Optical Astronomy Observatory, the national center for ground-based nighttime astronomy in the United States operated by the Association of Universities for Research in Astronomy (AURA) under cooperative agreement with the National Science Foundation.

This publication makes use of data products from the Wide-field Infrared Survey Explorer, which is a joint project of the University of California, Los Angeles, and the Jet Propulsion Laboratory/California Institute of Technology, and NEOWISE, which is a project of the Jet Propulsion Laboratory/California Institute of Technology. WISE and NEOWISE are funded by the National Aeronautics and Space Administration.

CasJobs was originally developed by the Johns Hopkins University/ Sloan Digital Sky Survey (JHU/SDSS) team. With their permission, MAST used version 3.5.16 to construct CasJobs-based tools for GALEX, Kepler, the Hubble Source Catalog, and PanSTARRS.

This research has made use of the SVO Filter Profile Service (http://svo2.cab.inta-csic.es/theory/fps/) supported from the Spanish MINECO through grant AyA2014-55216 The SVO Filter Profile Service[10] describes the Spanish VO Filter Profile Service. The Filter Profile Service Access Protocol. Rodrigo, C., Solano, E. http://ivoa.net/documents/Notes/SVOFPSDAL/index.html

APPENDIX A: QSO SAMPLE

In the submitted version of this paper, we had 463 QSOs selected from the literature which had $z \geq 5$, which we thought was the complete sample except a few that were published in 2019.

When we posted the submitted paper onto arXiv[11], we had two responses, one from Jinyi Yang, who pointed out that we missed QSOs in ? and Krisztina Perger, who also mentioned that we had missed *sim*40 QSOs and pointed us to her catalogue of QSOs[12]. We downloaded Tables 2,3 & 4 from ? using Vizier[13] and found all matches with $2''$ and added the remaining objects that had $z \geq 5$, one object from Table 3, SUHAWJ1016+2541, and 15 from Table 4, see Table A1. We also downloaded the 20190514 version of the Perger catalogue and X-matched that, finding all of the matches with $2''$ and looked for non-matches.

However, we spotted some inconsistences between the names of some of the QSOs in the Perger catalogue and decimal equatorial coordinates and pointed these out, and very rapidly Perger responded having fixed their catalogue. After further checks we found 10 objects (see Table A2) that were in both catalogues that there was disagreement on the coordinates. In some cases it was clear from the names that either we (Ross & Cross) had made a typo, or Perger had. In most other cases a search of the literature gave a clear answer. Two particular odd examples were SDSSJ0835+3227 and VA-13492, found in the Perger catalogue. In both cases the coordinates looked similar to SDSSJ0835+3217 and SDSSJ1040-1155 respectively and the redshifts were identical to these QSOs, which alerted us to a potential problem. These QSOs could be traced back in the literature: in the first case both QSOs are in ? and in the second case is VA-13492 is in ? which refers back to ? although the latter only seems to only contain SDSSJ1040-1155. In the case of SDSSJ0835+3227, we checked the SDSS-z band images[14], and found a bright source at the position of SDSSJ0835+3217 and no source at the position of SDSSJ0835+3227, see Figure A1. In the case of VA-13492, the I-band magnitude was equivalent to SDSSJ1040-1155 (I=25.9 mag), so we have decided that both of these objects have been transcribed incorrectly sometime in the past.

The objects from the submitted version of Ross

[10] Rodrigo, C., Solano, E., Bayo, A. http://ivoa.net/documents/Notes/SVOFPS/index.html
[11] http://www.arxiv.org
[12] http://astro.elte.hu/ perger/catalog.html
[13] http://vizier.u-strasbg.fr/
[14] https://dr15.sdss.org